Chinese Chemical Letters 37 (2026) 111002

Contents lists available at ScienceDirect

Chinese Chemical Letters

journal homepage: www.elsevier.com/locate/cclet

One-pot synthesis of Ni–Co nanoparticles@$Ni_{0.19}Co_{0.26}P$ nanowires core/shell arrays on Ni foam for efficient hydrogen evolution reaction at all pH values

Lei Zhang[a], Kaimin Chen[a], Luchang Li[a], Xiu Wei[a], Xianxin Cai[a], Yaohui Yu[a], Yixian Yang[a], Renping Cao[a], Fenghua Wei[a], Bang Lan[a], Yanhua Li[c,*], Xiaohu Luo[a], Hui Liang[a,*], Deshuai Zhen[b,*]

[a] *Northeast Guangdong Key Laboratory of New Functional Materials, Guangdong Rare Earth Photofunctional Materials Engineering Technology Research Center, Meizhou Rare Earth Photo functional Materials Engineering Technology Research Center, Office of Assets&Laboratory Management, School of Chemistry and Environment, Jiaying University, Meizhou 514015, China*

[b] *Hunan Key Laboratory of Typical Environment Pollution and Health Hazards, School of Public Health, Hengyang Medical School, University of South China, Hengyang 421001, China*

[c] *School of Materials Science and Engineering, Hunan Institute of Technology, Hengyang 421001, China*

ARTICLE INFO

Article history:
Received 17 December 2024
Revised 11 February 2025
Accepted 25 February 2025
Available online 26 February 2025

Keywords:
HER
pH-universal electrocatalyst
Non-precious
Core-shell structure
High conductivity

ABSTRACT

Developing non-precious electrocatalysts with high-efficiency hydrogen evolution reaction (HER) activity for hydrogen production at all pH values is crucial for the application and promotion of water electrolysis. Herein, a unique structure of nickel-cobalt (Ni–Co) nanoparticles@$Ni_{0.19}Co_{0.26}P$ nanowires core/shell arrays on Ni foam as a pH-universal electrocatalyst for hydrogen evolution is synthesized by a simple hydrothermal process and thermal reduction treatment. The morphological analysis reveals that numerous Ni–Co nanoparticles are densely packed inside the hollow interior of $Ni_{0.19}Co_{0.26}P$ nanowires. This unique structure integrates the advantages of high surface area from the nanowires and enhanced electronic conductivity from the Ni–Co nanoparticles, effectively addressing the conventional issue of slow charge transfer rate in 3D metal-based compounds, which is typically caused by a long transfer distance. The electrocatalysts provide an excellent hydrogen evolution reaction performance in alkaline, neutral, and acidic media with an overpotential of 35, 36, and 23 mV to reach the current density of 10 mA/cm^2, respectively. This study highlights the potential of Ni–Co nanoparticles@$Ni_{0.19}Co_{0.26}P$ nanowires as a cost-effective and pH-universal HER electrocatalyst, offering promising prospects for sustainable hydrogen production.

© 2026 Published by Elsevier B.V. on behalf of Chinese Chemical Society and Institute of Materia Medica, Chinese Academy of Medical Sciences.

Water electrolysis into green hydrogen has been regarded as a promising approach to alleviate the depletion of fossil fuels [1,2]. Electrocatalysts towards hydrogen evolution reaction (HER), one-half reaction in water electrolysis, are of significance for highly efficient hydrogen production in various conditions such as seawater, domestic and industrial sewage, and so forth [3,4]. The Pt-based catalysts can provide optimal performance in all pH values, but their high price and scarcity are not in conformity with the progress of the hydrogen energy economy [5,6].

With a lower price, non-precious metal-based compounds (phosphides, sulfides, nitrides, *etc.*) have attracted increasing attention [7,8]. Among them, transition metal phosphides (TMPs) have been considered potential candidates due to their ability to function well in both acidic and alkaline media for HER. Nonetheless, poor performance in neutral or basic media greatly hindered the applied range [9,10]. Tremendous efforts in the past few years promoted the performance improvements of TMPs for HER, even comparable to that of the Pt-based catalysts in acid and alkaline media [11,12], however, it is still up against the obstacles of low catalytic activity in neutral media. Plenty of accessible active sites and a fast charge transfer rate are the key factors for ideal electrocatalysts with high catalytic activity [13,14]. The design of three-dimensional (3D) structures with high surface area can achieve more accessible active sites[15,16]. Unfortunately, the charge always transfers more slowly in the 3D structure than that in 2D, 1D, and 0D due to a longer transfer distance [17,18]. The assembly of highly conductive components (metal quantum dots [19], conducting polymer [20], graphene [21], carbon materials [22], metal nanomaterials [23,24],

* Corresponding authors.
E-mail addresses: liyanhua87@hnu.edu.cn (Y. Li), lianghui861021@163.com (H. Liang), zhends.1987@163.com (D. Zhen).

https://doi.org/10.1016/j.cclet.2025.111002
1001-8417/© 2026 Published by Elsevier B.V. on behalf of Chinese Chemical Society and Institute of Materia Medica, Chinese Academy of Medical Sciences.

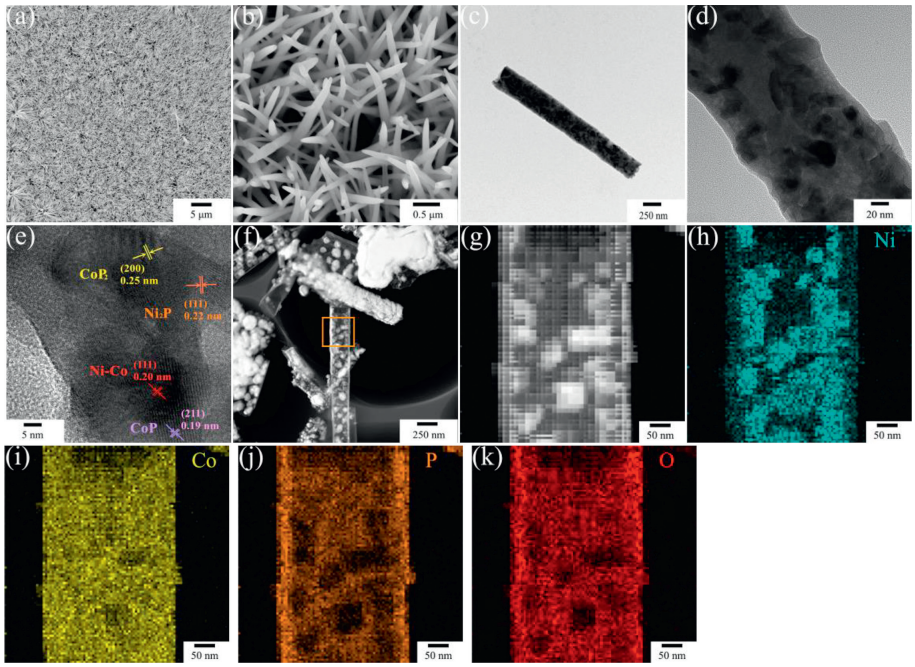


Fig. 1. Different magnifications of (a, b) SEM images and (c–e) TEM images, and (f–k) HAADF-STEM images and EDS mapping images of Ni–Co NPS@$Ni_{0.19}Co_{0.26}P$/NF.

etc.) into a 3D structure is a common strategy to facilitate charge transfer rate by synergy effect of the enhanced electronic conductivity and the regulated intrinsic activity. There are still several disadvantages: (1) Metal quantum dots at the nanoscale tend to aggregate by the nano-effect during intense HER, which results in poor stability. (2) The incorporation of supplementary conductive materials contributes to an increase in production costs. More efforts are required to address these disadvantages.

In this work, we report a novel approach for synthesizing Ni–Co nanoparticles@$Ni_{0.19}Co_{0.26}P$ nanowire core/shell arrays as electrocatalysts for hydrogen evolution reaction (HER) across all pH values, using a simple hydrothermal and thermal reduction treatment. The nanowire structure of the electrocatalyst provides a high surface area. More importantly, the nanowires feature a hollow interior filled with many stacked Ni–Co alloy nanoparticles, resulting in a significant enhancement in electrical conductivity. This unique structure eliminates the need for additional conductive materials, maintaining low cost while overcoming the issues of large surface area and suboptimal conductivity typically associated with 3D metal-based compounds. Consequently, the Ni–Co nanoparticles@$Ni_{0.19}Co_{0.26}P$ nanowire core/shell arrays demonstrate excellent HER activity and good stability across all pH values, comparable to that of Pt-based catalysts.

The nickel-cobalt (Ni–Co) nanoparticles (NPS)@$Ni_{0.19}Co_{0.26}P$ nanowires core/shell arrays on Ni foam (abbreviated as Ni–Co NPS@$Ni_{0.19}Co_{0.26}P$/NF) was synthesized by a hydrothermal process and subsequent thermal reduction treatment. The precursor material has a nanowire morphology with a diameter of about 200–250 nm and is uniformly covered on NF (Figs. S1a and b in Supporting information). The transmission electron microscopy (TEM) image also reveals a solid nanowire structure (Figs. S1c and d in Supporting information). During thermal reduction treatment, scanning electron microscopy (SEM) images (Figs. 1a and b) reveal that the material morphology remains unchanged, retaining its nanowire structures. Interestingly, TEM images present that the nanowires are hollow rather than solid, with numerous stacked nanoparticles filling the hollow interiors. The average particle size is 30 ± 0.716 nm (Figs. 1c and d). The lattice fringes with an interface distance of 0.20, 0.19, 0.22, and 0.25 nm (Fig. 1e) are assigned to the (111), (211), (111), and (200) planes of Ni (JCPDS No. 04-0850)-Co (JCPDS No. 15-0806) NPs, CoP (JCPDS No. 29-0497), Ni_2P (JCPDS No. 03-0953), and CoP_2 (JCPDS No. 26-0481), indicating that Ni–Co bimetal nanoparticles are formed insides its hollow interior. The high-angle annular diffraction field-scanning transmission electron microscopy (HAADF-STEM) images also suggest that hollow nanowires are filled by nanoparticles (Figs. 1f and g). Energy dispersive X-ray (EDX) images in Fig. 1h show a stronger Ni elements signal to appear at the location of the nanoparticle, while signals for P and O elements are absent or minimal (Figs. 1j and k). This suggests that the nanoparticles are primarily composed of Ni, with no detectable P or O. Additionally, the Co element exhibits a uniform distribution across the entire surface (Fig. 1i). These results imply alloyed Ni–Co nanoparticles are formed within the hollow nanowire structure, with a higher concentration of cobalt and a lower concentration of nickel.

To further validate this, the sample was investigated by X-ray diffraction (XRD) and X-ray photoelectron spectroscopy (XPS). As shown in Fig. 2, $Ni_2(CO_3)(OH)_2$ (JCPDS No. 35-0501) and $Co_2(CO_3)(OH)_2$ (JCPDS No. 48-0083) phases are observed in the precursor, while pure Ni (JCPDS No. 04-0850) and pure Co (JCPDS No. 15-0806) phases, Ni_2P (JCPDS No. 03-0953), CoP_2 (JCPDS No. 26-0481), and CoP (JCPDS No. 29-0497) phases can be discerned from Ni–Co NPS@$Ni_{0.19}Co_{0.26}P$/NF. This result strongly suggests the formation of Ni–Co nanoparticles, with the nanowires composed of Ni_2P, CoP_2, and CoP.

Peaks at 132.6, 532.7, 782.7, and 856.9 eV in the XPS survey spectrum (Fig. S2a in Supporting information) are attributed to P 2p, O 1s, Co 2p, and Ni 2p, respectively. Ni $2p_{3/2}$ and $2p_{1/2}$ XPS spectra (Fig. 3a) demonstrate the presence of metallic nickel (Ni^0) at ~852.7 and 869.8 eV, and Ni–P bonding at ~856.3 and 874.5 eV, with the satellite peak at ~862.3 and 880.1 eV [25], respectively. Co 2p XPS spectra (Fig. 3b) show the peaks at 778.2 and 793.2 eV, corresponding to Co $2p_{3/2}$ and $2p_{1/2}$ for metallic cobalt (Co^0), while peaks at ~781.3 and 797.3 eV are attributed to the Co–P bond, with satellite peaks at ~785.9 and 802.3 eV [26]. The P 2p XPS spectra (Fig. S2b in Supporting information) can be deconvo-

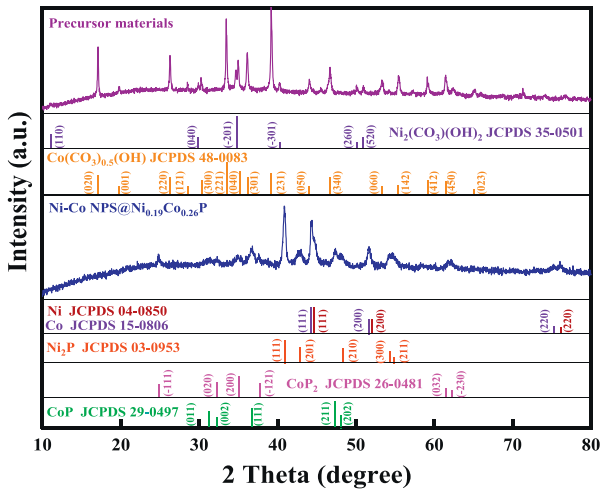


Fig. 2. XRD of the precursor materials and Ni–Co NPS@$Ni_{0.19}Co_{0.26}P$.

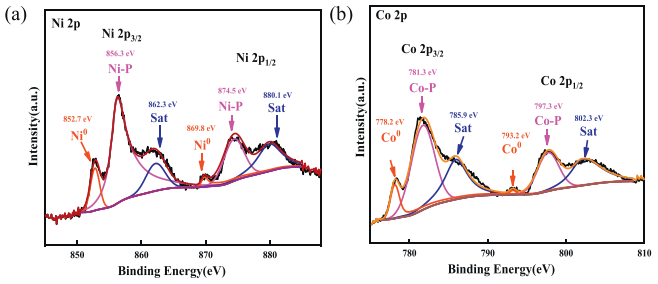


Fig. 3. High-resolution (a) Ni 2p, (b) Co 2p XPS spectra.

luted into three peaks at ~128.4, 129.1, and 133.7 eV corresponding to P $2p_{1/2}$, $2p_{3/2}$, and P–O, respectively, indicating the formation of metal phosphorus bond (M–P) and P–O bond. The O 1s XPS spectra (Fig. S2c in Supporting information) show a peak at 531.1 eV, associated with oxygen in the lattice, likely due to the oxidation of Ni_2P, CoP_2, and CoP in the air [27,28]. Their findings confirm the formation of Ni–Co nanoparticles (NPS) within the hollow nanowire structure, with the nanowires composed of Ni_2P, CoP_2, and CoP (denoted as Ni_xCo_yP). Additionally, the surface atomic ratios of Ni, Co, and P elements of Ni_xCo_yP are 0.56:0.36:1 by the XPS survey spectrum (Fig. S2a), respectively. The proportion of Ni in the Ni–P bond to Ni^0, and Co in the Co–P bond to Co^0 are 1:0.15 and 1:0.28 by the XPS Ni 2p and Co 2p (Figs. 3a and b), respectively. Therefore, the atomic ratio of Ni in the Ni–P bond and Co in the Co–P bond is 0.19:0.26, the Ni–Co nanoparticles (NPS)@Ni_xCo_yP can be abbreviated as Ni–Co NPS@ $Ni_{0.19}Co_{0.26}P$.

To reveal the role of the reducing agent (NaH_2PO_2) in the formation of Ni–Co NPS @$Ni_{0.19}Co_{0.26}P$ nanowires core/shell arrays, the precursors were calcined without the reducing agent. SEM and TEM images (Fig. S3 in Supporting information) reveal the formation of a nanowire structure but without a core/shell morphology. Ni, Co, and O elements are evenly distributed on the surface (Fig. S4 in Supporting information). The XRD result (Fig. S5 in Supporting information) shows only the $NiCo_2O_4$ phase (JCPDS No. 20-0781) with no other detectable phases. These suggest that the nanowire structure consists solely of $NiCo_2O_4$ when NaH_2PO_2 is absent, suggesting that NaH_2PO_2 is essential for the formation of Ni–Co nanoparticles (NPS) and the core/shell structure, consistent with previous reports [21,25]. On this basis, the formation mechanism of the unique structure can be described as follows. First, the precursor (Ni–Co)$_2$(CO$_3$)(OH)$_2$/Ni foam (NF) is prepared *via* a hydrothermal reaction (Eqs. S1-S3 in Supporting information). Then, (Ni–Co)$_2$(CO$_3$)(OH)$_2$/NF and NaH_2PO_2 are calcined at 400 °C for 3 h under a continuous flow of nitrogen (N_2) gas (Eqs. S4-S7 in Supporting information). During thermal decomposition, (Ni–Co)$_2$(CO$_3$)(OH)$_2$ releases CO_2 and H_2O (Eqs. S6 and S7 in Supporting information), with the gaseous products more readily escaping from the surface, resulting in a faster reaction rate at the surface compared to the interior. This creates a concentration gradient of –OH or CO_3^{2-} between the surface and interior of the (Ni–Co)$_2$(CO$_3$)(OH)$_2$ nanowires. Driven by this concentration difference, –OH and CO_3^{2-} ions move toward the surface, leading to the formation of a hollow nanowire structure. Similar exchanges occur between Ni^0/Co^0 and Ni^{2+}/Co^{2+}.

The Brunauer-Emmett-Teller (BET) specific surface area was investigated by N_2 adsorption-desorption measurements. For comparison, an irregular block structure Ni@Ni_2P/NF and a diamond block structure Co@Co_xP/NF were fabricated (details in Experiment process and Figs. S6-S9 in Supporting information). The specific surface area of Ni–Co NPS@$Ni_{0.19}Co_{0.26}P$/NF (Fig. S10 in Supporting information) is 18.5 m^2/g, nearly three times that of Ni@Ni_2P/NF (5.8 m^2/g) and Co@Co_xP/NF (6.3 m^2/g). A larger surface area has the advantage of better electrochemical reaction performance [29,30]. More importantly, the synthesized nanowires feature a hollow interior filled with Ni–Co nanoparticles, which greatly enhance electrical conductivity. This unique structure overcomes the charge transport limitations typically encountered in nanowires due to longer transport distances. As a result, the Ni–Co NPS@$Ni_{0.19}Co_{0.26}P$/NF architecture is expected to exhibit excellent performance in pH-universal hydrogen evolution reactions.

Furthermore, electrocatalytic properties for HER performances of samples were determined in alkaline (1 mol/L KOH), neutral (1 mol/L PBS), and acid (0.5 mol/L H_2SO_4) solutions, respectively. For comparison, $NiCo_2O_4$ core@Ni_xCo_yP shell nanowires on Ni foam are also prepared and estimated (Figs. S11-S14 in Supporting information). Fig. 4 displays LSVs, Tafel slope, and electrochemical impedance spectroscopy (EIS) curves, and the relevant values are shown in Tables S1-S3 (Supporting information). As shown in Figs. 4a–c, Ni–Co NPS@$Ni_{0.19}Co_{0.26}P$/NF provides an excellent HER performance in alkaline, neutral, and acid solutions with an overpotential of 35, 36, and 23 mV to reach the current density of 10 mA/cm^2 (η_{10}), respectively, even approximate to Pt/C (28, 32, 18 mV), much lower than those of Ni@Ni_2P/NF (101, 120, 93 mV), Co@Co_xP/NF (82, 95, 78 mV), $NiCo_2O_4$@Ni_xCo_yP/NF (145, 156, 133 mV), and Bare Ni foam (NF, 295, 380, 160 mV). Interestingly, all samples with metal nanoparticles (Ni–Co NPS@$Ni_{0.19}Co_{0.26}P$/NF, Ni@Ni_2P/NF, Co@Co_xP/NF) display much higher HER activity than $NiCo_2O_4$@Ni_xCo_yP/NF, because of their similar surface compositions, it seems to be implying that a better pH-universal HER activity is dominated by the formed metal nanoparticles insides samples rather than their surface activity. This should be attributed to their enhanced conductivity by the formed metal nanoparticles, resulting in a faster charge transfer rate. To further confirm this point, the charge transfer rate and impedance were investigated by the Tafel slope and EIS. As shown in Figs. 4d–f, the Tafel slope of Ni–Co NPS@$Ni_{0.19}Co_{0.26}P$/NF is the smallest among samples, except for Pt/C (Table S1), suggesting a more favorable charge transfer rate on the Ni–Co NPS@$Ni_{0.19}Co_{0.26}P$/NF in pH-universal electrolyte. By fitting Nyquist plots in Figs. 4g–i, R_{ct} values of Ni–Co NPS@$Ni_{0.19}Co_{0.26}P$/NF in alkaline, neutral, and acid solutions are determined to be 3.52, 5.55, 2.34 Ω, which is significantly better as compared to Ni@Ni_2P/NF, Co@Co_xP/NF, $NiCo_2O_4$ @Ni_xCo_yP/NF, and NF (Table S1). These demonstrate that Ni–Co NPS@ $Ni_{0.19}Co_{0.26}P$/NF has a stronger charge transfer ability in pH-universal electrolytes for HER. The electrochemical surface area (ECSA) was obtained by the relative double-layer capacitance (Figs. S15-S20 in Supporting information). Notably, ECSA

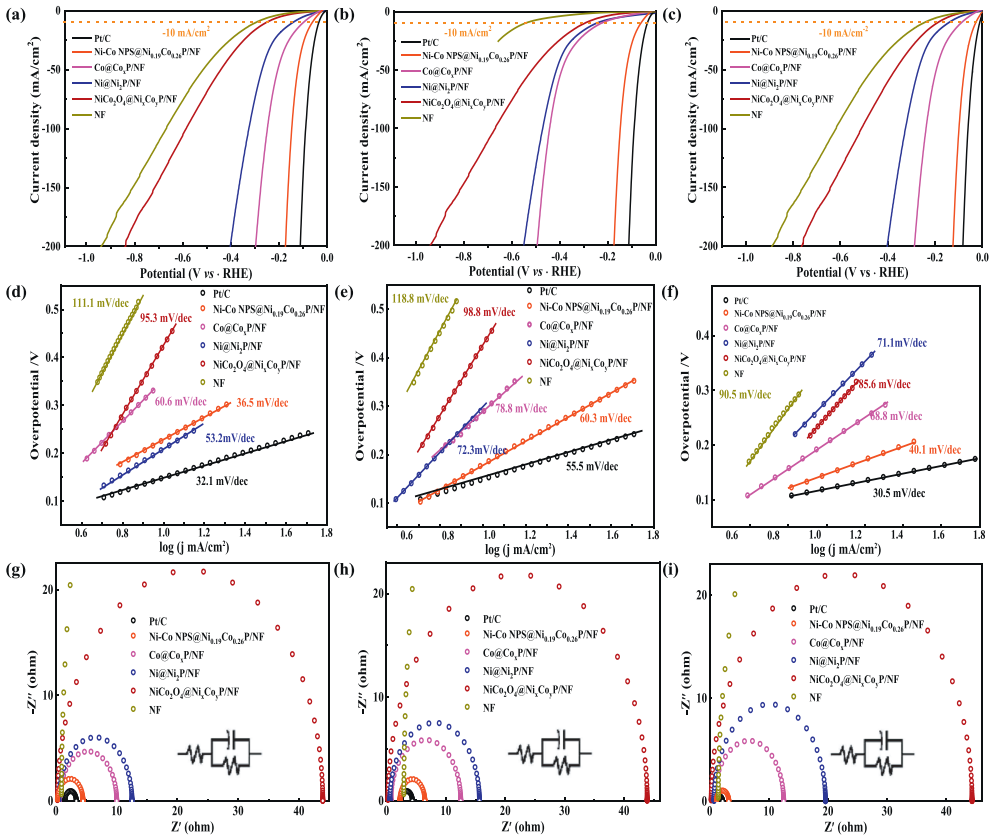


Fig. 4. (a–c) LSVs, (d–f) Tafel slope curves, (g–i) the fitted Nyquist plots of the electrocatalysts in alkaline (1 mol/L KOH), neutral (1 mol/L PBS), and acid (0.5 mol/L H_2SO_4) solutions.

of $NiCo_2O_4$@Ni_xCo_yP/NF is close to Ni–Co NPS@$Ni_{0.19}Co_{0.26}$P/NF, which is about 10-fold larger than Ni@Ni_2P/NF and Co@Co_xP/NF (Table S1). However, the normalized LSVs by ECSA (Fig. S21 in Supporting information) suggest a more favorable HER activity on the Ni–Co NPS@$Ni_{0.19}Co_{0.26}$P/NF, Ni@Ni_2P/NF, and Co@Co_xP/NF than $NiCo_2O_4$@ Ni_xCo_yP/NF, which is consistent with the above. Thus, the boosted HER activity in pH-universal should be attributed to high electric conductivity rather than the electrode surface activity. The Ni–Co nanoparticles within the hollow interior of Ni–Co NPS@$Ni_{0.19}Co_{0.26}$P/NF contribute to the favorable HER performance by enhancing conductivity. Meanwhile, Ni–Co NPS@$Ni_{0.19}Co_{0.26}$P/NF also demonstrates good stability (Fig. S22 in Supporting information).

In conclusion, we report a straightforward method for synthesizing unique core/shell arrays of Ni–Co Nanoparticles@$Ni_{0.19}Co_{0.26}$P nanowires on Ni foam as a pH-universal electrocatalyst for hydrogen evolution. The morphological analysis reveals that nanowires present a hollow interior structure, which is filled with numerous nanoparticles. XRD analysis confirms the presence of Ni_2P, CoP_2, and CoP phases in the nanowires, while XPS analysis, based on element ratios, identifies the mixed phase as $Ni_{0.19}Co_{0.26}$P. EDX, XRD, and XPS results further suggest that the nanoparticles are composed of pure Ni and Co. The nanowire structure provides a high surface area, and the Ni–Co nanoparticles enhance the material's electrical conductivity. Due to the synergistic effects of these components, the Ni–Co NPS@$Ni_{0.19}Co_{0.26}$P/NF electrocatalyst demonstrates excellent hydrogen evolution reaction performance across alkaline, neutral, and acidic media, with overpotentials of 35, 36, and 23 mV, respectively, at a current density of 10 mA/cm^2, comparable to Pt-based catalysts.

Declaration of competing interest

The authors declare that they have no known competing financial interests or personal relationships that could have appeared to influence the work reported in this paper.

CRediT authorship contribution statement

Lei Zhang: Writing – review & editing, Writing – original draft, Visualization, Validation, Supervision, Software, Resources, Project administration, Methodology, Investigation, Funding acquisition, Formal analysis, Data curation, Conceptualization. **Kaimin Chen:** Formal analysis, Data curation. **Luchang Li:** Formal analysis, Data curation. **Xiu Wei:** Formal analysis, Data curation. **Xianxin Cai:** Formal analysis, Data curation. **Yaohui Yu:** Formal analysis, Data curation. **Yixian Yang:** Formal analysis, Data curation. **Renping Cao:** Writing – original draft. **Fenghua Wei:** Investigation. **Bang Lan:** Funding acquisition. **Yanhua Li:** Investigation, Funding acquisition. **Xiaohu Luo:** Writing – original draft. **Hui Liang:** Writing – original draft. **Deshuai Zhen:** Writing – review & editing, Writing – original draft.

Acknowledgments

This work is financially supported by a Special Fund (Climbing Plan) for Guangdong Province's Science and Technology Innovation Strategy in 2024 (No. Pdjh2024b351). University Engineering Technology Center of Guangdong (No. 2022GCZX007). Inorganic Optical Functional Materials and Application Innovation Team of Guangdong (No. 2023KCXTD033). Department of Education of Guangdong Province (No. 2021KQNCX087). The Natural Science Foundation of

China (No. 42307369). The University Key Laboratory of Guangdong (No. 2024KSYS021). Scientific Research Fund of Hunan Provincial Education Department (No. 22B0864).

Supplementary materials

Supplementary material associated with this article can be found, in the online version, at doi:10.1016/j.cclet.2025.111002.

References

[1] M. Rezayeenik, M. Mousavi-Kamazani, S. Zinatloo-Ajabshir, Appl. Phys. A 129 (2023) 47.
[2] M.S. Alnarabijia, O. Tantawib, A. Ramlic, et al., Renew. Sust. Energ. Rev. 114 (2019) 109326.
[3] H. Li, X. Zi, J. Wu, et al., Nano Res. 18 (2025) 94907146.
[4] F.A. Garcés-Pineda, M. Blasco-Ahicart, D. Nieto-Castro, et al., Nat. Energy 4 (2019) 519.
[5] F. Yu, L. Yu, I.K. Mishra, et al., Mater. Today Phys. 7 (2018) 121–138.
[6] Q. Wang, Y. Gong, Y. Tan, et al., Chin. J. Catal. 54 (2023) 229–237.
[7] C. Cai, K. Liu, L. Zhang, et al., Angew. Chem. Int. Ed. 62 (2023) e202300873.
[8] M. Cao, K. Liu, Y. Song, et al., J. Energy Eng. 72 (2022) 125–132.
[9] Z. Guo, Y. Cui, W. Liu, ACS Catal. 14 (2024) 9413–9420.
[10] M. Xing, S. Zhu, X. Zeng, et al., Adv. Energy Mater. 13 (2023) 2302376.
[11] R. Zhang, X.X. Wang, S.J. Yu, Adv. Mater. 29 (2017) 1605502.
[12] Y. Mo, Y. Ni, X. Li, et al., Int. J. Hydrogen Energy 48 (2023) 31101–31109.
[13] C. Cai, K. Liu, Y. Zhu, Angew. Chem. Int. Ed. 61 (2022) e202113664.
[14] Z. Wang, B. Xiao, Z. Lin, et al., Angew. Chem. Int. Ed. 60 (2021) 23388.
[15] J. Liu, J. Jiang, C. Cheng, et al., Adv. Mater. 23 (2011) 2075.
[16] W. Xiong, X. Pan, Y. Li, et al., Mater. Lett. 157 (2015) 23.
[17] Y. Dong, T. Slade, M.J. Stolt, et al., Angew. Chem. Int. Ed. 56 (2017) 14453.
[18] R.R. Devarapalli, S. Szunerits, Y. Coffinier, et al., ACS Appl. Mater. Interfaces 8 (2016) 4298.
[19] Z. Chen, H. Xu, Y. Ha, et al., Appl. Catal. B: Environ. 250 (2019) 213–223.
[20] R. Liu, S.B. Lee, J. Am. Chem. Soc. 130 (2018) 2942.
[21] M.B. Zakaria, Y. Guo, J. Na, et al., ChemSusChem 13 (2020) 3269–3276.
[22] D. Zhen, C. Liu, Q. Deng, et al., Chin. Chem. Lett. 35 (2024) 109249.
[23] Y. Zhao, M. Luo, S. Chu, et al., Nano Energ. 59 (2019) 146.
[24] D. Zhen, S. Zhang, A. Yang, et al., Int. J. Biol. Macromol. 259 (2024) 129104.
[25] D. Zhang, J. Shi, Y. Qi, Adv. Sci. 5 (2018) 1801216.
[26] Y. Men, P. Li, J. Zhou, et al., ACS Catal. 9 (2019) 3744–3752.
[27] C. Tang, L. Gan, R. Zhang, et al., Nano Lett. 16 (2016) 6617–6621.
[28] J. Kibsgaard, C. Tsai, K. Chan, et al., Energy Environ. Sci. 8 (2015) 3022–3029.
[29] C.K. Chan, H. Peng, G. Liu, et al., Nat. Nanotechnol. 3 (2008) 31.
[30] Y. Xia, P. Yang, Y. Sun, et al., Adv. Mater. 15 (2003) 353.